Title	Finite-width feed and load models
Author(s)	Lo, YH; Jiang, LJ; Chew, WC
Citation	IEEE Transactions On Antennas And Propagation, 2013, v. 61 n. 1, p. 281-289
Issued Date	2013
URL	http://hdl.handle.net/10722/182790
Rights	Creative Commons: Attribution 3.0 Hong Kong License

Finite-Width Feed and Load Models

Yat Hei Lo, Li Jun Jiang, *Member, IEEE*, and Weng Cho Chew, *Fellow, IEEE*

***Abstract*—We demonstrate a new method of applying the feed model for the method of moments (MoM) formulation for the electric field integral equation (EFIE). The model is based around a previously reported magnetic ribbon current model which is accurate and allows for a finite width of the feed port. However, with proper approximations, one can reduce the formulation such that the magnetic field operator can be removed in order to simplify computations arising from the curl of the dyadic Green's function and its singularities. We show here that the new feed model can also be used to model a lumped element.**

***Index Terms*—Delta-gap source, EFIE, input impedance, magnetic-current source, variational formula.**

I. Introduction

THE study of wire antennas and antennas of arbitrary shape has always been an important topic, where intensive research has been consistently carried out [1]–[4]. The modeling of wire antennas, antennas of arbitrary shapes, and many circuit designs involve the requirement of a source or feed model. Regarding the construction of the feed model, there has been compromise between the accuracy and simplicity to the formulations applied. One of the most common formulations used is the electric-field integral equation (EFIE) together with the method of moments (MoM) [5]. In most cases for MoM, a delta-gap feed model is used. The excitation is considered as a small port, where its gap width is assumed to be zero. When using the Rao–Wilton–Glisson (RWG) basis function set [6], the feed port becomes a voltage jump across a set of edges that assemble the delta-gap. Although unphysical, this feed model allows very simple implementation of the source [7], and therefore is very commonly applied.

However, the delta-gap is nonideal since no physical feed can have zero gap. The port impedance, for example, can be far from accurate when the feed is assumed to have zero gap width. Efforts to model a more realistic feed port has been made [8]–[11].

Manuscript received March 16, 2012; accepted August 20, 2012. Date of publication August 24, 2012; date of current version December 28, 2012. This work was supported in part by the Research Grants Council of Hong Kong (GRF 711609, 711508, 711511, and 713011), HKU Small Project Funding (201007176196), HKU Seed funding (201102160033), HKU UDF-CSE grant, and in part by the University Grants Council of Hong Kong (Contract No. AoE/P-04/08).

Y. H. Lo and L. J. Jiang are with the Department of Electrical and Electronic Engineering, University of Hong Kong, China (e-mail: yhlo@eee.hku.hk; ljiang@eee.hku.hk).

W. C. Chew was with the Department of Electrical and Electronic Engineering, University of Hong Kong. He is now with the Department of Electrical and Computer Engineering, University of Illinois at Urbana-Champaign, Urbana, IL 61801 USA (e-mail: wcchew@hku.hk).

Color versions of one or more of the figures in this paper are available online at http://ieeexplore.ieee.org.

Digital Object Identifier 10.1109/TAP.2012.2215294

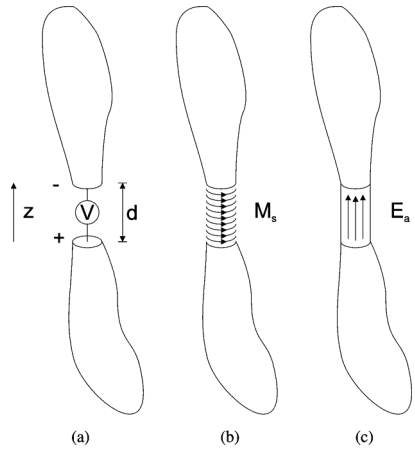

Fig. 1. Equivalent excitation models for a voltage applied at a feed port.

An accurate feed model shall be one that is derived from the equivalence principle [12]. An ideal voltage source is equivalent to enclosing the feed port with a circulating magnetic ribbon current, while filling the gap of the port by PEC [8]. An accurate model based on this magnetic ribbon current formulation is numerically demonstrated in [9]. Since magnetic current is involved, the excitation is calculated using the magnetic-field operator, or the $\mathcal{K}$-operator [13]. The singularity treatment of the $\mathcal{K}$-operator [14] is also required since the magnetic ribbon resides on the surface of the feed port. This increases the complexity and difficulty of implementation.

In this paper, we start from the accurate model based on the magnetic ribbon current presented in [9]. The excitation can be further simplified as an incident electric field that lies on the surface of the feed port. This way, we remove the implementation of the $\mathcal{K}$-operator, and, hence, the formulation becomes more friendly to EFIE. The new model allows a finite width of the feed port. Moreover, this model can be modified to allow one to insert lumped passive load elements with a finite width. The lumped elements are essentially the current-dependent voltage source. We also demonstrate here that using variational formulation of the input impedance, the convergence of any iterative solver can be accelerated.

II. Formulation

Consider an arbitrary PEC object as shown in Fig. 1(a), where the feed port is essentially a voltage that is applied at the gap. The voltage source is equivalent to shorting the gap with a thin wire enclosed by a circulating magnetic ribbon current [8]. As far as the value of the voltage is concerned, the wire can be as wide as the gap itself such that the entire gap can be filled with PEC like a thick wire, as shown in Fig. 1(b), with the magnetic ribbon current that circulates around it.

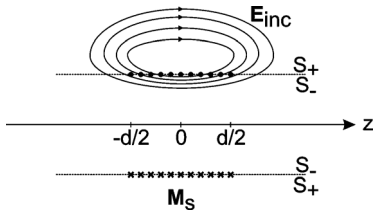

Fig. 2. Electric field generated by the magnetic ribbon current around the feed gap.

The magnetic ribbon is analogous to the case of an electric solenoid, where a circulating magnetic current produces an electric field. The electric field produced inside the gap is thus the incident field for the EFIE formulation. We denote the magnetic ribbon current as $\mathbf{M}_s$ and the electric field inside the gap as $\mathbf{E}_a$. Then, their relation is given by [9]

$$\mathbf{M}_s = -\hat{n} \times \mathbf{E}_a \tag{1}$$

where $\hat{n}$ is the unit surface normal vector. The values of $\mathbf{M}_s$ and $\mathbf{E}_a$ can be determined from the applied voltage given by

$$V_{\text{in}} = \int_{-d/2}^{d/2} E_z dz \tag{2}$$

across the feed port. In [9], $\mathbf{M}_s$ is assumed to be uniform across the gap, provided that d is much smaller than the wavelength. Hence

$$\mathbf{M}_s = -\hat{n} \times \hat{z} \frac{V_{\text{in}}}{d}. \tag{3}$$

The choice of such uniform $\mathbf{M}_s$ provides a proper incident field where (2) is valid. Using $\mathbf{M}_s$, the excitation for the EFIE can be determined using the magnetic field Green's function and the $\mathcal{K}$-operator as

$$\mathbf{E}_{\text{inc}}(\mathbf{r}) = \nabla \times \int_S dS' \, \overline{\mathbf{G}}(\mathbf{r}, \mathbf{r}') \cdot \mathbf{M}_s(\mathbf{r}') \tag{4}$$

where $\overline{\mathbf{G}}(\mathbf{r}, \mathbf{r}')$ is the dyadic Green's function.

The electric field generated by the magnetic ribbon is analogous to the case of an electric solenoid, where an electric current loop generates a circulating magnetic field around it. Here, a series of magnetic current loops around the feed generates an electric field, as illustrated in Fig. 2. One can determine the z-component of the electric field just inside and just outside the ribbon, denoted by S_- and S_+, respectively, which are shown in Fig. 3. It can be shown that

$$\int_{-\infty}^{\infty} E_{z,\text{inc}} dz = 0, \quad \text{on } S_+ \tag{5}$$

$$\int_{-\infty}^{\infty} E_{z,\text{inc}} dz = -\int_{-\infty}^{\infty} M_\phi dz = -V_{\text{in}}, \quad \text{on } S_- \tag{6}$$

where the integral of the z-component of the electric field along S_- yields the voltage applied at the feed gap. The same integral along S_+ shall be zero.

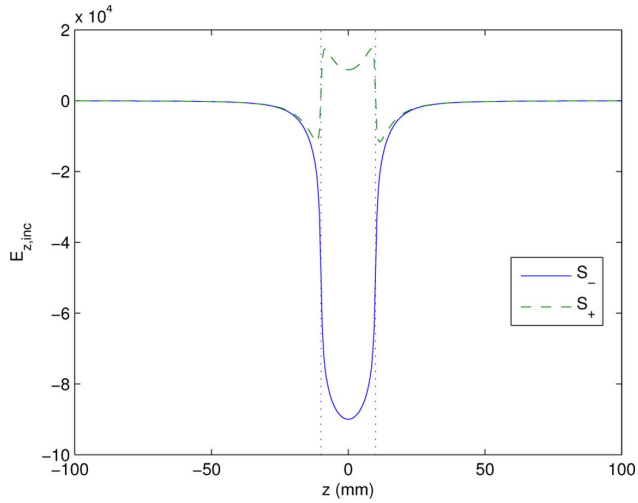

Fig. 3. Electric field along z-direction just inside (S_-) and just outside (S_+) the magnetic ribbon.

The $E_{z,\text{inc}}$ at S_- becomes the excitation field on the PEC, and it will induce a current on the PEC that produces $\mathbf{E}_{\text{sca}}$ to exactly cancel $E_{z,\text{inc}}$ on the surface, i.e., $E_{z,\text{tot}} = 0$ on the PEC surface. One can show that

$$\int_{-\infty}^{\infty} E_{z,\text{sca}} dz = V_{\text{in}}. \tag{7}$$

For a PEC cylinder with a constant radius of a, the EFIE of the scattering of the cylinder driven by a ribbon current is given by

$$-E_{z,\text{inc}} = i2\pi a\omega\mu\hat{z} \cdot \int_{-\infty}^{\infty} \overline{\mathbf{G}}(z, z') \cdot \mathbf{J}_p(z') dz' = E_{z,\text{sca}} \tag{8}$$

where $E_{z,\text{inc}}$ is the incident electric field generated by the magnetic ribbon current on S_- as given by (4). In the weak form, the above becomes

$$\begin{aligned} &-\langle T_j(z), E_{z,\text{inc}}(z) \rangle \\ &\quad = i\omega\mu \left\langle T_j(z), 2\pi a\hat{z} \cdot \int_{-\infty}^{\infty} \overline{\mathbf{G}}(z, z') \cdot \mathbf{J}_p(z') dz' \right\rangle \\ &\quad = \langle T_j(z), E_{z,\text{sca}}(z) \rangle \end{aligned} \tag{9}$$

where T_j is a set of testing or weighting function, and $j = 1, 2, \ldots, N$.

In the weak form, $E_{z,\text{inc}}$ does not have to be exactly equal to $E_{z,\text{sca}}$, but they are equal to each other in the weighted sense when tested by $T_j(z)$. The most important physics of the ribbon current is to induce a voltage drop given by (6), and hence the current that produces a voltage rise given by (7). To calculate $E_{z,\text{inc}}$ using (4), it is often difficult due to the curl operator on the Green's function and its singularity. It is also time consuming since the incident field over the entire object is calculated. However, from Fig. 3, one can approximate the $E_{z,\text{inc}}$ on S_- to a more easily defined function and yet suffices to produce

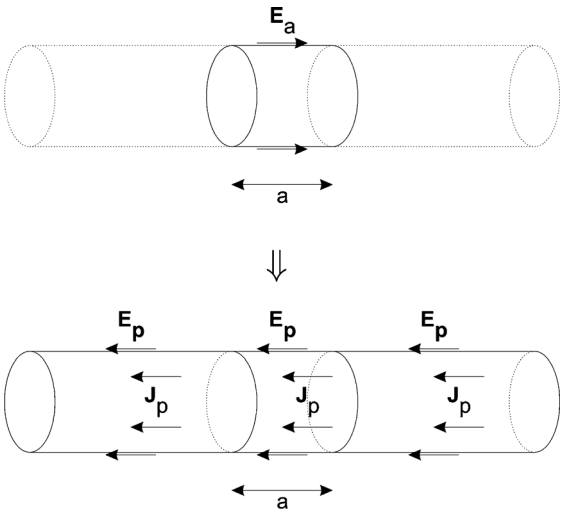

Fig. 4. The excitation field (top) and the corresponding induced current and electric field (bottom) of an antenna excited by a uniform field as the finite-width feed. a denotes the feed (aperture) region.

the required voltage. One simple function would be the pulse function defined as

$$E_{z,a} = E_{z,\mathrm{inc}} = \begin{cases} \frac{V}{d}, & -\frac{d}{2} \le z \le \frac{d}{2} \\ 0, & \text{otherwise} \end{cases} \tag{10}$$

since $E_{z,\mathrm{inc}}$ and $E_{z,\mathrm{sca}}$ are sufficiently localized near $z = 0$, as seen from Fig. 3. The above definition of $E_{z,\mathrm{inc}}$ truncates the incident field into the gap area and still results in the validity of (6) and (7), i.e., the integral of the incident field across the vicinity of the feed equals the voltage applied.

The general EFIE is given by

$$-E_{z,a} = i2\pi a\omega\mu\hat{z}\cdot \int_{-\infty}^{\infty} \overline{\mathbf{G}}(z,z')\cdot\mathbf{J}_p(z')dz' \tag{11}$$

where $E_{z,a} = V/d$ and $-(d/2) \le z \le (d/2)$, similarly defined using (10).

III. Variational Formula for Input Admittance

One way to determine the input impedance of an antenna is to calculate the ratio between the applied voltage and the current that flows across the gap. It might be more straightforward to determine the input admittance. Fig. 4 shows the antenna where the region a denotes the feed gap or aperture. $\mathbf{E}_a$ denotes the uniform incident electric field that is defined at the aperture only. After the induced current $\mathbf{J}_p$ is solved for, the input admittance is given by

$$Y_{\mathrm{in}} = \frac{I}{V} = \frac{\langle \mathbf{E}_a, \mathbf{J}_p \rangle}{V^2} \tag{12}$$

where $\mathbf{J}_p$ is the induced current, which generates $\mathbf{E}_p$, the scattered electric field that cancels the incident field $\mathbf{E}_a$ at the aperture.

The above is a direct form of the input admittance, which is not variational. To make it variational, an additional term is introduced. This additional term shall be zero when $\mathbf{J}_p$ is exact. Hence, (12) becomes

$$Y_{\mathrm{in}} = \frac{\langle \mathbf{E}_a, \mathbf{J}_p \rangle}{V^2} + \frac{\langle \mathbf{E}_t, \mathbf{J}_p \rangle}{V^2} \tag{13}$$

where $\mathbf{E}_t$ is the total electric field, given by

$$\mathbf{E}_t = \mathbf{E}_a + \mathbf{E}_p \tag{14}$$

where $\mathbf{E}_a$ is the incident field and $\mathbf{E}_p$ is the scattered field. For an exact solution, the scattered field shall exactly cancel the incident field. Hence, $\mathbf{E}_t$ is zero and does not affect the value of Y_{in}.

To prove that (13) is variational, we take the first-order variation about the exact solution, which becomes

$$\delta Y_{\mathrm{in}} \approx \frac{1}{V^2}\left(\langle \mathbf{E}_a, \delta\mathbf{J}\rangle + \langle \mathbf{E}_{te}, \delta\mathbf{J}\rangle + \langle \delta\mathbf{E}, \mathbf{J}_{pe}\rangle\right) \tag{15}$$

where the additional subscript e denotes exact solutions. By reciprocity, we have

$$\langle \delta\mathbf{E}, \mathbf{J}_{pe}\rangle = \langle \mathbf{E}_{pe}, \delta\mathbf{J}\rangle. \tag{16}$$

Using (16) and (14), (15) can be written as

$$\begin{aligned} \delta Y_{\mathrm{in}} &\approx \frac{1}{V^2}\left(\langle \mathbf{E}_a, \delta\mathbf{J}\rangle + \langle \mathbf{E}_{te}, \delta\mathbf{J}\rangle + \langle \mathbf{E}_{pe}, \delta\mathbf{J}\rangle\right) \\ &= \frac{2}{V^2}\langle \mathbf{E}_{te}, \delta\mathbf{J}\rangle \\ &= 0. \end{aligned} \tag{17}$$

The above is true because the exact solution $\mathbf{E}_{pe}$ completely cancels $\mathbf{E}_a$ tangentially and results in zero $\mathbf{E}_{te}$. Hence, when a first-order error of $\mathbf{J}_p$ exists, the error of Y_{in} remains zero to the first order. This variational formulation yields a more accurate calculation of the input admittance, thereby the input impedance. In many cases when iterative solver is used, it can also reduce the number of iterations as long as the input impedance is considered. Using (14), (13) can also be written as

$$Y_{\mathrm{in}} = 2\frac{\langle \mathbf{E}_a, \mathbf{J}_p \rangle}{V^2} + \frac{\langle \mathbf{E}_p, \mathbf{J}_p \rangle}{V^2} \tag{18}$$

where $\langle \mathbf{E}_p, \mathbf{J}_p \rangle$ is readily obtained from the MoM matrix system itself. Hence, the above form for determining Y_{in} requires little additional computation.

IV. Lumped Impedance (Load) Elements

For most models involving circuits or antennas, one needs to introduce additional passive elements such as capacitors, inductors, or resistors in a distributive network. For example, resistors and capacitors are often used to suppress reflections and impedance matching. In general, it is equivalent to inserting lumped elements into the model with given impedance values to each element.

Previously, the lumped elements were modeled in a similar fashion as the delta-gap feed port [15]. An element with an infinitesimally small width is inserted, which causes a voltage drop across the associated edges. Since the voltage drop is dependent on the current, the elements in the impedance matrix corresponding to lumped elements are modified accordingly. In this method, the current and voltage drops are both associated with the same basis function that assembles the delta-gap lumped element. Hence, only some of the diagonal elements in the MoM matrix are affected.

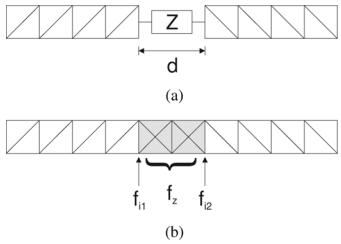

Fig. 5. Equivalent lumped element model with a finite width.

Here in our formulation, the treatment for the lumped element is similar to that of the finite-width feed port. A finite-width element is considered as a port that causes a voltage drop given by

$$V_g = Z_g I_g \tag{19}$$

where Z_g is the impedance of the lumped element; I_g is the current that flows through the element. As with the case of the feed port, the lumped element is replaced by closed PEC, as shown in Fig. 5. We consider the case of the method of moments using the RWG basis and Galerkin testing [6], where $\mathbf{J}_p$ is expressed as

$$\mathbf{J}_p \approx \sum_{n=1}^{N} I_n \mathbf{f}_n(\mathbf{r}) \tag{20}$$

where $\mathbf{f}_n(\mathbf{r})$ is the RWG basis function. While a lumped element is inserted, there exist two special sets of basis functions: $\mathbf{f}_z$, which is within the region of the lumped element, and $\mathbf{f}_i$, which is the edge connecting the lumped element and the normal PEC outside the gap. This is illustrated in Fig. 5(b), where the shaded area indicates the position of the lumped element. Here, $\mathbf{f}_z$ are the basis functions within this shaded area, and $\mathbf{f}_i$ are those edges at the boundary between the shaded and unshaded areas.

Recall that the voltage V_g depends on the current I_g, in turn J_p, which is the unknown to be solved for. This means that the excitation vector is dependent on the unknown itself. Hence, the terms in the excitation vector that are associated with lumped elements are corrected by introducing additional terms in the corresponding elements in the impedance matrix. To do so, one should first notice that the current flowing across the element is given by

$$I_g = \sum_i I_i l_i = \sum_i I_g^i \tag{21}$$

at either end of the element, where l_i and I_i are the corresponding edge length and the coefficient of basis functions. From Fig. 5(b), the current can be determined from either $\mathbf{f}_{i1}$ or $\mathbf{f}_{i2}$. Their values shall be equal for gaps of small widths, i.e., the current entering the element is equal to that of leaving the element. This follows from the current continuity. Given $V_g = Z_g I_g$, and $E_{z,g} = V_g/d$, assuming the current flows along the z axis, then for every entry in the impedance matrix $\overline{\mathbf{Z}}$, where $\mathbf{f}_z$ and $\mathbf{f}_i$ intersect, the value of the matrix entry is corrected by

$$Z_{zi} \to Z'_{zi} = Z_{zi} + \frac{1}{I_i}\langle \mathbf{f}_z, E_{z,g}\hat{z}\rangle \tag{22}$$

$$= Z_{zi} + \frac{1}{I_i}\left\langle \mathbf{f}_z, \frac{Z_g I_g^i}{d}\hat{z}\right\rangle \tag{23}$$

$$= Z_{zi} + \left\langle \mathbf{f}_z, \frac{Z_g l_i}{d}\hat{z}\right\rangle \tag{24}$$

before the matrix is solved. Notice the factor $1/I_i$ in the above equation is inserted since I_i has been used to weight the unknown J_i of the MoM system.

A. Lumped Elements With Loop-Tree Decomposition

The EFIE breaks down at very low frequencies. This is very common for most circuit and electrically small structure problems. It is because when (11) is applied, the EFIE operator ($\mathcal{L}$-operator) is broken into two terms given by [13]

$$\begin{aligned}\mathcal{L}_E\mathbf{J}_s &= i\omega\mu\int_S dS'\overline{\mathbf{G}}(\mathbf{r},\mathbf{r}')\mathbf{J}_s(\mathbf{r}')\\ &= i\omega\mu\int_S dS' g(\mathbf{r},\mathbf{r}')\mathbf{J}_s(\mathbf{r}')\\ &\quad + \frac{1}{i\omega\epsilon}\nabla\int_S dS' g(\mathbf{r},\mathbf{r}')\nabla'\cdot\mathbf{J}_s(\mathbf{r}')\end{aligned} \tag{25}$$

where $g(\mathbf{r},\mathbf{r}')$ is the scalar Green's function. The first term above is due to vector potential, and the second term comes from the scalar potential, and is also called the charge term. It can be seen that for low frequencies, the second term dominates. However, there exists $\mathbf{J}_s(\mathbf{r}')$ such that $\nabla'\cdot\mathbf{J}_s = 0$ and resulting in a null-space. The eigenvalues of the second term are very large or zero while the eigenvalues of the first term are small. Hence, the matrix becomes ill-conditioned.

One way to overcome this issue is to apply the loop-tree decomposition, frequency normalization, and basis rearrangement. These procedures are done to improve the condition of the matrix, and thus can be regarded as applying a sequence of pre- and postconditioning matrices. The resulting system is then solved using an iterative solver.

When decomposing the original matrix containing the RWG basis set into the matrix containing the loop-tree basis set, the following operation is performed [16]:

$$\overline{\mathbf{Z}}_{\mathrm{LoopTree}} = \overline{\mathbf{F}}_{\mathrm{LTR}}\cdot\overline{\mathbf{Z}}^{V}_{\mathrm{RWG}}\cdot\overline{\mathbf{F}}^{t}_{\mathrm{LTR}} + \begin{bmatrix}\overline{\mathbf{0}} & \overline{\mathbf{0}}\\ \overline{\mathbf{0}} & \overline{\mathbf{F}}_{\mathrm{TR}}\cdot\overline{\mathbf{Z}}^{S}_{\mathrm{RWG}}\cdot\overline{\mathbf{F}}^{t}_{\mathrm{TR}}\end{bmatrix} \tag{26}$$

where

$$\overline{\mathbf{Z}}_{\mathrm{LoopTree}} = \begin{bmatrix}\overline{\mathbf{Z}}_{\mathrm{LL}} & \overline{\mathbf{Z}}_{\mathrm{LT}}\\ \overline{\mathbf{Z}}_{\mathrm{TL}} & \overline{\mathbf{Z}}_{\mathrm{TT}}\end{bmatrix} \tag{27}$$

$$\begin{bmatrix}\mathbf{J}_L(\mathbf{r})\\ \mathbf{J}_T(\mathbf{r})\end{bmatrix} = \overline{\mathbf{F}}_{\mathrm{LTR}}\cdot\mathbf{J}_{\mathrm{RWG}}(\mathbf{r}) \tag{28}$$

$$\overline{\mathbf{F}}_{\mathrm{LTR}} = \begin{bmatrix}\overline{\mathbf{F}}_{\mathrm{LR}}\\ \overline{\mathbf{F}}_{\mathrm{TR}}\end{bmatrix}. \tag{29}$$

Here, $\overline{\mathbf{Z}}^{V}_{\mathrm{RWG}}$ contains only the first (vector potential) term and $\overline{\mathbf{Z}}^{S}_{\mathrm{RWG}}$ contains only the second (scalar potential) term from (25). $\overline{\mathbf{F}}_{\mathrm{LR}}$ and $\overline{\mathbf{F}}_{\mathrm{TR}}$ are connection matrices that convert the RWG basis set to loop and tree basis sets. For a system with N_{RWG} RWG basis functions (unknowns), then it is always true that

$$N_L + N_T = N_{\mathrm{RWG}} \tag{30}$$

where N_L and N_T are the number of loop bases and tree bases, respectively. Hence, $\overline{\mathbf{F}}_{\mathrm{LR}}$ has a dimension of $N_L \times N_{\mathrm{RWG}}$, $\overline{\mathbf{F}}_{\mathrm{TR}}$ has a dimension of $N_T \times N_{\mathrm{RWG}}$, and $\overline{\mathbf{F}}_{\mathrm{LTR}}$ has a dimension of $N_{\mathrm{RWG}} \times N_{\mathrm{RWG}}$, same as that of the impedance matrices $\overline{\mathbf{Z}}_{\mathrm{RWG}}$ and $\overline{\mathbf{Z}}_{\mathrm{LoopTree}}$. In (26), any $\nabla' \cdot \mathbf{J}_s$ within the RWG basis set that forms a loop is zero. In another word, any matrix element in $\overline{\mathbf{Z}}_{\mathrm{LoopTree}}$ that contains a loop basis has its $\nabla' \cdot \mathbf{J}_s$ equal to zero.

From (24), if there exists any lumped elements, one needs to insert the correction term for the lumped element into the impedance matrix. Essentially, this is equivalent to adding an additional term into the corresponding entries in $\overline{\mathbf{Z}}_{\mathrm{RWG}}$. When constructing $\overline{\mathbf{Z}}_{\mathrm{LoopTree}}$; however, $\overline{\mathbf{Z}}_{\mathrm{RWG}}$ is decomposed into two matrices $\overline{\mathbf{Z}}^V_{\mathrm{RWG}}$ and $\overline{\mathbf{Z}}^S_{\mathrm{RWG}}$. The correction term can be inserted into only one of the two matrices. It can be seen that $\overline{\mathbf{Z}}^S_{\mathrm{RWG}}$ only connects to the block $\overline{\mathbf{Z}}_{\mathrm{TT}}$ for tree-tree bases interaction. It does not completely contribute to $\overline{\mathbf{Z}}_{\mathrm{LoopTree}}$. On the other hand, $\overline{\mathbf{Z}}^V_{\mathrm{RWG}}$ connects to the entire $\overline{\mathbf{Z}}_{\mathrm{LoopTree}}$ using $\overline{\mathbf{F}}_{\mathrm{LTR}}$. Therefore, it is appropriate to insert lumped element correction terms in $\overline{\mathbf{Z}}^V_{\mathrm{RWG}}$, and through $\overline{\mathbf{F}}_{\mathrm{LTR}}$, the correction values are included into the correct entries of the newly constructed impedance matrix, $\overline{\mathbf{Z}}_{\mathrm{LoopTree}}$.

V. Radiation From Feed

It is interesting to note that, in common practice, one considers the radiation of an antenna solely from the electric field generated by the currents on the antenna only. It was never considered that the feed itself is also radiating. Previous formulations do not allow study of the radiation from the feed since it was modeled as a nonphysical voltage jump only. Here, when the feed is formulated around a finite width, it is straightforward to determine its radiation.

To benchmark the radiation of the antenna, the radiation pattern is compared between the field generated from the antenna and the feed. The radiation pattern is determined from its far-field radiation. For a dipole antenna along the z axis, the electric far-field radiation pattern on the x–z plane is given by

$$|E_\theta(\theta)|^2 = \left(\frac{\omega\mu}{4\pi r}\right)^2 \left|\hat{\theta}\cdot \int_S e^{-i\mathbf{k}\cdot\mathbf{r}'}\mathbf{J}(\mathbf{r}')d\mathbf{r}'\right|^2 \qquad (31)$$

where $\mathbf{k} = k\hat{r}$, $\hat{r} = \hat{x}\sin\theta + \hat{z}\cos\theta$, and $\phi = 0$. The above is derived from the first term of (25) with some approximation due to far-field calculations. Moreover, in common practice, the field pattern is normalized against its maximum. Therefore, the coefficient outside the integral is not considered, especially when r tends to infinity. At the feed, when only magnetic ribbon current is considered as the source, the electric far-field pattern is given by

$$|E_\theta(\theta)|^2 = \left(\frac{k}{4\pi r}\right)^2 \left|\hat{\theta}\cdot \int_S e^{-i\mathbf{k}\cdot\mathbf{r}'}\left[\hat{r}\times\mathbf{M}_a(\mathbf{r}')\right]d\mathbf{r}'\right|^2. \qquad (32)$$

Once the model is set up and the resultant MoM problem is solved for, (31) and (32) can be used to determine the contribution of the radiated field from the antenna itself and the feed using magnetic ribbon current.

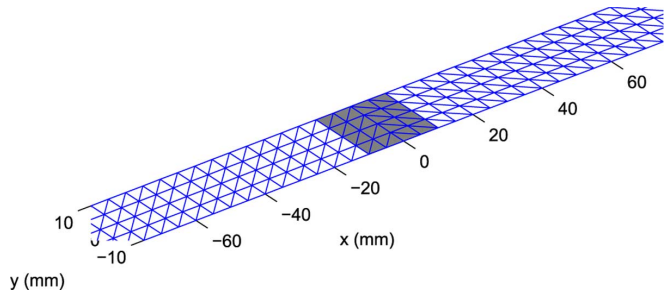

Fig. 6. Section of the strip antenna model.

TABLE I
Values of Z_{in} of a Half-Wavelength Strip Dipole

Feed model	Z_{in} (Ω)
New feed model	$87.35 + 52.56j$
Delta-gap	$88.68 + 51.82j$
Reference models [7]	Z_{in} (Ω)
MoM, RWG, delta-gap, 244-triangle mesh	$88 + 47j$
Wire with 19 segments	$90 + 53j$
WIPL-D simulation	$85 + 44j$

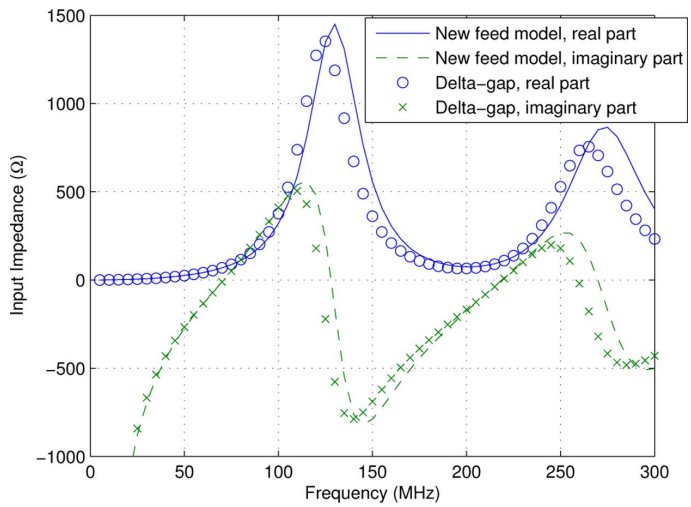

Fig. 7. Input impedance of the half-wavelength strip dipole.

VI. Numerical Results

A. Strip Antenna With Single Feed

We first verify our formulation using a half-wavelength dipole antenna. The antenna is a strip of 2-m length and 20-mm width. A section of the strip is shown in Fig. 6, where it is modeled as an open surface. The feed port is located at the center of the strip, denoted by the shaded region. In this case, it shows a feed port of 20-mm width. The corresponding working frequency is 75 MHz. We compare both delta-gap and our finite-width models. Table I shows the value of the input impedance determined from different models, also shown are some values previously reported [7] for comparison. Our new model is consistent with the delta-gap model where the values fall within the range previously presented.

Fig. 7 shows the input impedance of the dipole over a range of frequencies up to 300 MHz. Results from both the finite-width

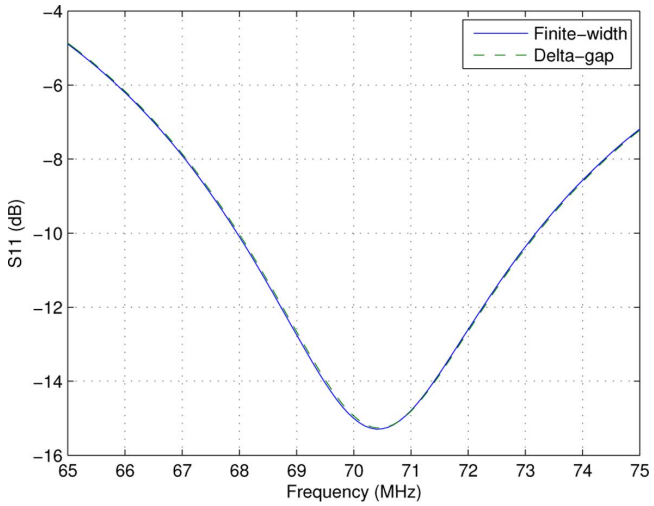

Fig. 8. S11 of the half-wavelength strip dipole.

feed and delta-gap feed are shown. Due to the finite width of the strip, the resonant frequency is expected to be slightly lower than 75 MHz. We can see using the S11 graph of the antenna shown in Fig. 8. Our result indicates that the first resonant wavelength is about 70.4 MHz. Moreover, one usually operates the antenna at a frequency where the reactance diminishes, i.e., $\Im m[Z_{\rm in}] = 0$. In general, it happens when the length of the antenna is about $l = 0.47\lambda$ to 0.48λ [10]. It was found in our case that when $\Im m[Z_{\rm in}] = 0$, the frequency is around 70.7 MHz, which agrees well from prediction, and is consistent with both the new finite-width and delta-gap feeds.

B. Cylindrical Structures

There are many cases when the delta-gap feed model fails to provide an accurate result. For example, when determining the impedance of a feed port, the width of the port greatly affects the calculation result. Here, we show a cylindrical structure with a feed applied at the center. With this model, we show different dimensions of a cylinder that correspondingly represent a half-wavelength dipole antenna, a parallel disk capacitor, and others.

Table II shows the input impedance of the cylinder functioning as a half-wavelength wire antenna, along with an equivalent model to the case of the strip dipole described in case A. The cylinder has a 2-m length and 5-mm radius. The operating frequency is 75 MHz. We show different width of the feed port from 10 to 40 mm. A more accurate feed model using magnetic ribbon current [9] is also applied for comparison. As can be seen, there is a clear dependence of the port impedance on the width of the feed port. The result is consistent between the new finite-width feed and the ribbon current feed. The delta-gap feed model, however, does not handle the finite width of the feed and hence cannot properly determine the port impedance of a physical feed port.

It is interesting to note that in [7], it states that a strip antenna model is equivalent to a corresponding wire model with $w = 4a$, where w is the width of the strip, and a is the radius of the wire. Here, comparing the values in Tables I and II, the discrepancy between the wire and strip models are obvious. However, as a quick measure and the approximation of the antenna parameter, the strip model may still be convenient in many cases since it involves much fewer unknowns than the wire model. The wire model should be used in cases where higher accuracy is required.

TABLE II
VALUES OF $Z_{\rm in}$ OF A HALF-WAVELENGTH WIRE DIPOLE

Feed width (mm)	$Z_{\rm in}$ (Ω)	
	New feed model	Ribbon current
10	$87.59 + 49.23j$	$87.10 + 49.53j$
20	$87.15 + 49.50j$	$86.86 + 49.67j$
30	$86.85 + 49.68j$	$86.65 + 49.80j$
40	$86.63 + 49.83j$	$86.47 + 49.92j$
Delta-gap	$89.11 + 48.27j$	

TABLE III
VALUES OF $Z_{\rm in}$ OF A SHORT WIRE OF LENGTH 100 mm, CALCULATED FROM FINITE-WIDTH FEED AND RIBBON CURRENT FEED

Feed width (mm)	$Z_{\rm in}$ (Ω)	
	New feed model	Ribbon current
10	$0.119 - 2.31 \times 10^3 j$	$0.155 - 2.64 \times 10^3 j$
20	$0.157 - 2.67 \times 10^3 j$	$0.186 - 2.90 \times 10^3 j$
30	$0.190 - 2.97 \times 10^3 j$	$0.216 - 3.17 \times 10^3 j$
40	$0.222 - 3.26 \times 10^3 j$	$0.248 - 3.45 \times 10^3 j$
Delta-gap	$0.045 - 1.42 \times 10^3 j$	

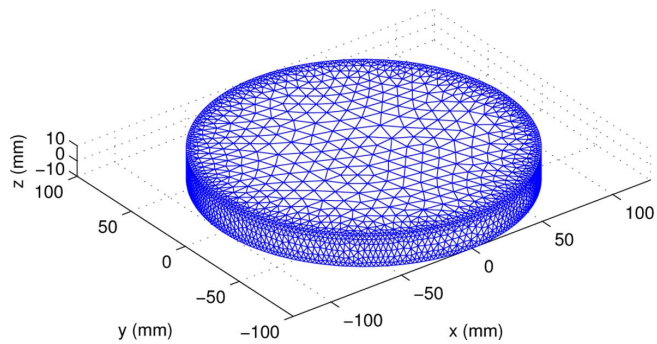

Fig. 9. A parallel-plate capacitor modeled with the finite-width feed excitation. The entire gap between the two plates are closed and filled with PEC.

When the cylinder becomes shorter, the effect of the feed size becomes more significant. Table III shows the same wire antenna but with a length that is just 100 mm. In this case, the delta-gap feed results in an input impedance of $(0.045 - 1.42 \times 10^3 j)\Omega$, which is far from the results obtained from the finite-width feed and the magnetic ribbon current models. Again, as the width of the feed varies, the impedance changes accordingly. The delta-gap is unable to show the effect of the feed width.

Fig. 9 shows another cylindrical configuration that represents a parallel disk capacitor. Using the new finite-width feed model, it appears as a thin solid circular disk since the gap area is also filled with PEC. The corresponding model using delta-gap should be created as the one shown in Fig. 10, where a strip is used to connect the two disks (as the highlighted region shown), and a delta-gap is fed at the center of the strip. This is the common practice of modeling such parallel-plate configuration using a delta-gap. The radii of the disks are 100 mm, and they are separated by 20 mm. The expected value of the capacitance of this model is 18.347 pF [17]. Using a frequency of 1 kHz,

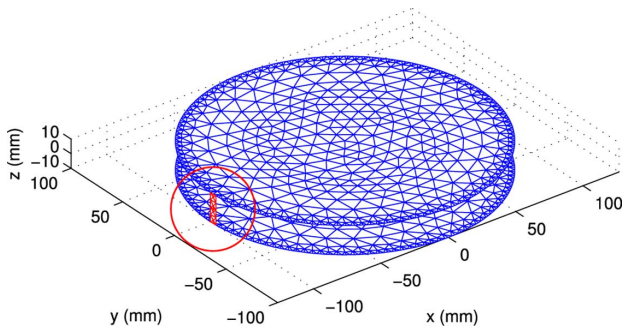

Fig. 10. The parallel-plate capacitor modeled with the delta-gap excitation. A small strip is inserted to connect the two disks, with a delta-gap at the middle of the strip.

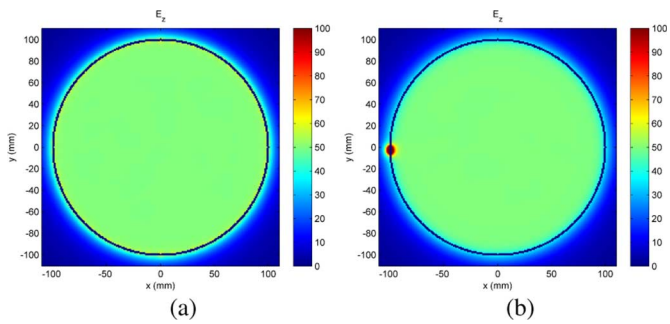

Fig. 11. The electric field inside the parallel plate capacitor calculated from the two models of feed. The blue rim indicates the edge of the parallel plates. (a) From the finite-width feed and (b) from the delta-gap feed.

and the low-frequency treatment as mentioned before [18], the capacitance determined using the new finite-width feed and the delta-gap models are 18.315 and 18.189 pF, respectively. In this case, the configuration of the delta-gap can accurately model the capacitance of the parallel plate.

For the case of the delta-gap excitation, although the feed is applied at a small section of the edge of the plate, instead of uniformly around the plate as in the case of the new feed model, the resultant electric field in between the parallel plate is indeed uniform. This is shown in Fig. 11. The delta-gap does result in a spot of very strong electric field around the feed. However, it does not affect the electric-field distribution overall. The value of capacitance calculated using the delta-gap feed is also reasonably close to the theoretical prediction, although not as accurate as that of the new finite-width feed model. Therefore, it has been accepted as the common practice of capacitance calculation using the delta-gap. Note, however, that there must be a strip being set up to connect the air space between the two plates. This is not easily feasible for many other cases such as the antenna shown previously, since it generates edges attached to more than two triangular patches and creates nonindependent basis functions. Hence, it causes more complexity when modeling other structures using delta-gap on strips. Note also that in this case, when one applies the ribbon current model as in Fig. 9, the incident electric field resulting from the ribbon current changes rapidly around the edge of the disk. This rapid change of the incident field causes breakdown of the MoM formulation and thus cannot provide a correct result. The finite-width feed model, however, does not have such problem.

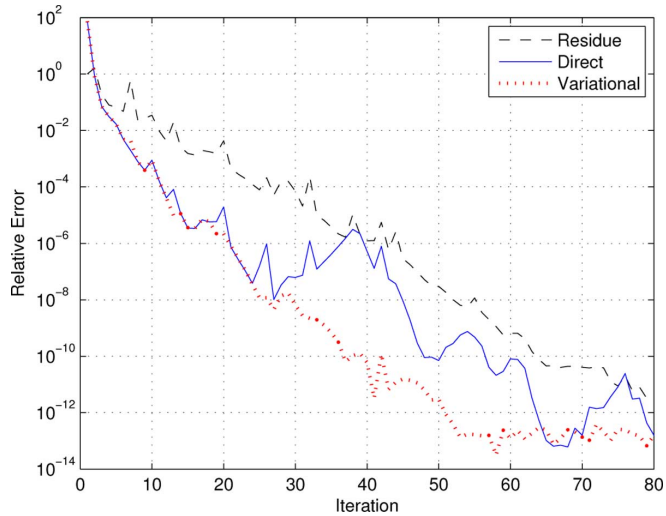

Fig. 12. Convergence of the input impedance of the half-wavelength strip dipole model using BiCG iterative solver, loop-tree decomposition, and variational formulation.

C. Variational Formulation

The basis elements in the strip antenna are small compared to the wavelength. When using iterative solvers, the problem is best solved with loop-tree decomposition, frequency normalization, and basis rearrangement. This results in a well-conditioned matrix system requiring greatly reduced number of iterations. Here, we used the bi-conjugate gradient (BiCG) method as the iterative solver. The value of the input impedance is calculated during each iteration using the variational form given in (18), as well as the direct form given in (12) for comparison. Fig. 12 shows the convergence of the BiCG solver. In addition to the relative residue shown in Fig. 12, the relative error of the input impedance to the exact value are shown for comparison. The input impedance is calculated from the direct form (labeled as Direct) using (12) and the variational form (labeled as Variational) using (18). The exact value of the input impedance is calculated using direct LU decomposition. In this problem, the matrix system contains 1010 unknowns.

Fig. 12 shows the expected behavior of BiCG, where the residual decreases reasonably monotonically. Due to the use of the low-frequency treatment, convergence can be easily achieved within 100 iterations. It can be seen that the convergence of Z_{in} using variational formulation is much faster than that of the residual, where the relative error of Z_{in} reaches a minimum within 60 iterations. Moreover, the variational formulation enhances the accuracy of the value of input impedance by at least two orders of magnitude compared to the direct form. In addition, the direct form shows larger fluctuation because it is more susceptible to inaccuracies from machine precision.

D. Finite-Width Lumped Elements

To demonstrate the implementation of the lumped elements formulation, we take the same half-wavelength strip dipole as used previously. A pair of 100-Ω resistors of 20-mm lengths are inserted at ±0.5 m, that is, centered between the feed port and each ends. With the two loads introduced, the input impedance at 75 MHz is determined. Table IV shows the resultant input

TABLE IV
VALUES OF Z_{in} FOR A LOADED STRIP DIPOLE

Feed/Load Models	Z_{in} (Ω)
New feed model	$193.44 - 0.317j$
Delta-gap	$191.83 - 7.25j$
Equivalent wire monopole [7]	$198 + 0.1j$

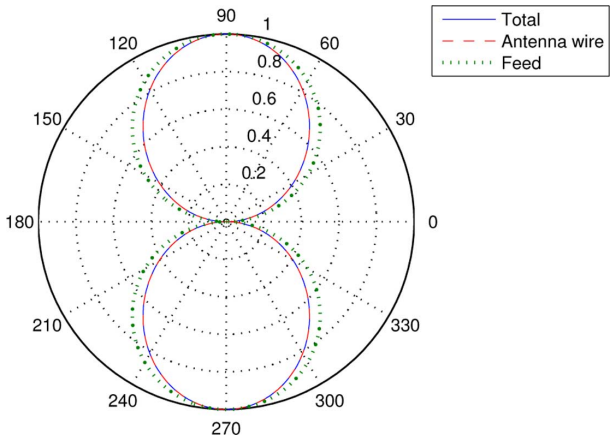

Fig. 13. Normalized radiation patterns of a half-wavelength dipole antenna, and its 20-mm feed.

impedances determined from different models. Again, the calculations from the new finite-width feed and load models are consistent with the delta-gap models. The results also show that the values are closer to that of the reference given by [7].

E. Radiation Patterns

In order to analyze the contribution of the radiation arising from the feed, the radiation patterns from the antenna and the feed were determined separately. Here, we apply a 20-mm feed to the half-wavelength dipole antenna of length 2 m. Fig. 13 shows the typical radiation pattern of such antenna. The forward direction of radiation is at 0° and 180°. It is shown that the radiation pattern from the antenna and the feed are slightly different. The radiation pattern of the antenna is equivalent to the analytical form of a line antenna with a sinusoidal current distribution given by [19]

$$\mathbf{E} = -\hat{\theta}\frac{i\eta I_m e^{ikr}}{2\pi r}\left[\frac{\cos(kl\cos\theta) - \cos kl}{\sin\theta}\right]. \tag{33}$$

On the other hand, due to the small size of the magnetic ribbon feed, the radiation pattern is shown to have the same form as a Hertzian dipole, which has the form

$$\mathbf{E} = -\hat{\theta}i\omega\mu Il\frac{e^{ikr}}{4\pi r}\sin\theta. \tag{34}$$

Again, the antenna radiation is defined as the electric field generated from the electric current J of the antenna given by (31). The feed radiation is the electric field generated by the magnetic ribbon current of the feed, given by (32). Fig. 14 shows the ratio of the forward radiation between two cases, over a frequency range of up to 300 MHz.

The operation frequency of the antenna is around 75 MHz. At this frequency, the radiation from the antenna is over 90 dB stronger than that from the feed. The radiation from the antenna is more than 60 dB higher than the feed up to at least the third

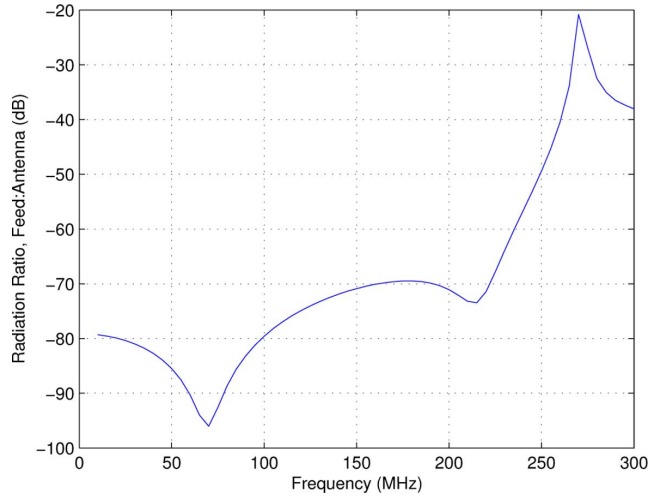

Fig. 14. Ratio of the forward radiation by the feed and the half-wavelength dipole antenna.

harmonics (225 MHz). The result shows that for the case of the object acting as a radiating antenna, the radiation from the feed can be safely ignored, which is the general practice. In many cases when the structure is smaller than the wavelength, the feed radiation may also be negligible. However, from Fig. 14, over the extreme cases where the frequency is very high, the effect from the feed starts to become significant. Its radiation should also be considered.

VII. CONCLUSION

In this paper, we have presented a new model for the feed ports for the purpose of an antenna or circuit design system. The formulation is based on a variational form around the EFIE and the MoM. A more accurate model uses a physical finite-width gap and lumped elements. The simplicity of the new model compared to the previous models avoids the requirement of the implementation of the magnetic field operator and its singularities. At the same time, it can capture the effect of a finite feed width to the port impedance. Moreover, it allows implementation of lumped load elements easily. The new feed and load models are compatible with the low-frequency treatment for integral equation, namely the loop-tree decomposition, frequency normalization, and basis rearrangement. Using variational formulation, one can speed up calculations with an iterative solver by reducing the number of iterations required, due to the higher accuracy of the variational form of the equation. We have shown that with the new model, we can achieve better accuracy compared to the conventional delta-gap source and faster convergence.

ACKNOWLEDGMENT

The authors would like to thank N. Wong, Q. Dai, and Y. Chen for many discussions and code debugging, and S. He for advice on iterative solver issue.

REFERENCES

[1] R. King and C. W. Harrison, "The distribution of current along a symmetrical center-driven antenna," *Proc. IRE*, vol. 31, no. 10, pp. 548–567, Oct. 1943.

[2] C. T. Tai, "A new interpretation of the integral equation formulation of cylindrical antennas," *IRE Trans. Antennas Propag.*, vol. 3, no. 3, pp. 125–127, Jul. 1955.
[3] J. Richmond, "A wire-grid model for scattering by conducting bodies," *IEEE Trans. Antennas Propag.*, vol. 14, no. 6, pp. 782–786, Nov. 1966.
[4] C. Butler and D. Wilton, "Analysis of various numerical techniques applied to thin-wire scatterers," *IEEE Trans. Antennas Propag.*, vol. 23, no. 4, pp. 534–540, Jul. 1975.
[5] R. F. Harrington, *Field Computation by Moment Methods*. New York: MacMillan, 1968.
[6] S. Rao, D. Wilton, and A. Glisson, "Electromagnetic scattering by surfaces of arbitrary shape," *IEEE Trans. Antennas Propag.*, vol. 30, no. 3, pp. 409–418, May 1982.
[7] S. N. Makarov, *Antenna and EM Modeling With Matlab*. New York: Wiley, 2002.
[8] E. C. Jordan and K. G. Balmain, *Electromagnetic Waves and Radiating Systems*. Englewood Cliffs, NJ: Prentice-Hall, 1968.
[9] T. J. Cui and W. C. Chew, "Accurate model of arbitrary wire antennas in free space, above or inside ground," *IEEE Trans. Antennas Propag.*, vol. 48, no. 4, pp. 482–493, Apr. 2000.
[10] C. A. Balanis, *Antenna Theory Analysis and Design*. New York: Wiley, 2005.
[11] R. Maaskant and M. Arts, "Reconsidering the voltage-gap source model used in moment methods," *IEEE Antennas Propag. Mag.*, vol. 52, no. 2, pp. 120–125, Apr. 2010.
[12] R. F. Harrington, *Time-Harmonic Electromagnetic Fields*. New York: McGraw-Hill, 1961.
[13] W. C. Chew, M. S. Tong, and B. Hu, *Integral Equation Methods for Electromagnetic and Elastic Waves*. San Rafael, CA: Morgan & Claypool, 2009.
[14] P. Yla-Oijala and M. Taskinen, "Calculation of cfie impedance matrix elements with RWG and $n \times \mathrm{RWG}$ functions," *IEEE Trans. Antennas Propag.*, vol. 51, no. 8, pp. 1837–1846, Aug. 2003.
[15] D. Jiao and J.-M. Jin, "Fast frequency-sweep analysis of RF coils for MRI," *IEEE Trans. Biomed. Eng.*, vol. 46, no. 11, pp. 1387–1390, Nov. 1999.
[16] W. C. Chew, J. M. Jin, E. Michielssen, and J. Song, *Fast and Efficient Algorithms in Computational Electromagnetics*. Norwood, MA: Artech House, 2000.
[17] W. C. Chew and J. A. Kong, "Asymptotic formula for the capacitance of two oppositely charged discs," *Math. Proc. Camb. Philos. Soc.*, vol. 89, no. 02, pp. 373–384, 1981.
[18] J.-S. Zhao and W. C. Chew, "Integral equation solution of maxwell's equations from zero frequency to microwave frequencies," *IEEE Trans. Antennas Propag.*, vol. 48, no. 10, pp. 1635–1645, Oct. 2000.
[19] J. A. Kong, *Electromagnetic Wave Theory*. New York: Wiley, 1986.

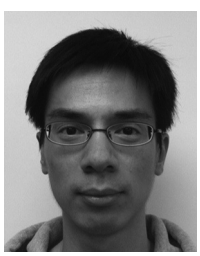

Yat Hei Lo received the B.Tech. degree in optoelectronics, the M.Sc. degree in physics, and the Ph.D. degree in physics, all from the Physics Department from the University of Auckland, New Zealand, in 2003, 2004, and 2009, respectively.

During the period in Auckland, his research interest was around optical interferometry, spectroscopy and imaging, from visible optics to Terahertz (T-ray) beams. He is currently a Postdoctoral Research Fellow at the Department of Electrical and Electronic Engineering in the University of Hong Kong. His research interests include computational electromagnetic modeling, integral equation methods, low frequency algorithms, and nanoantenna assisted optical effects.

Li Jun Jiang (S'01–M'04) received the B.S. degree in electrical engineering from the Beijing University of Aeronautics and Astronautics, China, in 1993, the M.S. degree from the Tsinghua University, China, in 1996, and the Ph.D. degree from the University of Illinois at Urbana-Champaign in 2004.

From 1996 to 1999, he was an Application Engineer with the Hewlett-Packard Company. Since 2004, he has been the Postdoctoral Researcher, Research Staff Member, and the Senior Engineer at IBM T. J. Watson Research Center. Since the end of 2009, he has been an Associate Professor with the Department of Electrical and Electronic Engineering at the University of Hong Kong. His research interests focus on electromagnetics, EMC/EMI, antennas, multidisciplinary EDA solutions, RF and microwave technologies, and high-performance computing (HPC), etc.

Dr. Jiang received the HP STAR Award in 1998. In 2003, he received the IEEE MTT Graduate Fellowship Award, and in 2004 the Y. T. Lo Outstanding Research Award. In 2008, he received the IBM Research Technical Achievement Award. He was the Semiconductor Research Cooperation (SRC) Industrial Liaison for several academic projects. Since 2009, he has been the SRC Packaging High Frequency Topic TT Chair. He has served as the Technical Committee Member for IEEE EDAPS since 2010, the Scientific Committee Member of 2010 IEEE SMEE, and the Associate Guest Editor of IEEE PROCEEDINGS since 2011. He also serves as the reviewer of many primary electromagnetics journals and special sessions organizers for many international conferences.

Weng Cho Chew (S'79–M'80–SM'86–F'93) received the B.S. degree in 1976, both the M.S. and Engineer's degrees in 1978, and the Ph.D. degree in 1980, all in electrical engineering from the Massachusetts Institute of Technology, Cambridge.

He served as the Dean of Engineering at The University of Hong Kong, Hong Kong, from 2008 to 2011. He was a Professor and the Director of the Center for Computational Electromagnetics and the Electromagnetics Laboratory, the University of Illinois at Urbana-Champaign, Urbana-Champaign. Before joining the University of Illinois at Urbana-Champaign, he was the Department Manager and a Program Leader at Schlumberger-Doll Research, Cambridge. He is the originator of several fast algorithms for solving electromagnetics scattering and inverse problems. He has led a research group that has developed parallel codes to solve dense matrix systems with tens of millions of unknowns for the first time for integral equations of scattering. He has authored a book titled *Waves and Fields in Inhomogeneous Media* (New York: IEEE Press, 1999), coauthored two books titled *Fast and Efficient Methods in Computational Electromagnetics* (Boston, MA: Artech House, 2001) and *Integral Equation Methods for Electromagnetic and Elastic Waves* (San Rafael, CA: Morgan & Claypool, 2007, 1st ed.), authored or coauthored more than 300 journal publications, more than 400 conference publications, and more than ten book chapters. His research interests include the areas of waves in inhomogeneous media for various sensing applications, integrated circuits, microstrip antenna applications, and fast algorithms for solving wave scattering and radiation problems.

Dr. Chew served on the IEEE Adcom for Antennas and Propagation Society as well as on the Geoscience and Remote Sensing Society. He has been active with various journals and societies. He is the Fellow of the Optical Society of America, the Institute of Physics, the Electromagnetics Academy, and the Hong Kong Institute of Engineers, and was the National Science Foundation Presidential Young Investigator. He received the Schelkunoff Best Paper Award for the IEEE TRANSACTIONS ON ANTENNAS AND PROPAGATION (AP), the IEEE Graduate Teaching Award, the UIUC Campus Wide Teaching Award, and the IBM Faculty Awards. He was a Founding Professor of the College of Engineering, and previously, the First Y. T. Lo Endowed Chair Professor in the Department of Electrical and Computer Engineering, University of Illinois at Urbana-Champaign. From 2005 to 2007, he served as an IEEE Distinguished Lecturer. He served as the Cheng Tsang Man Visiting Professor at Nanyang Technological University, Singapore, in 2006. In 2002, the Institute for Science Information Citation elected him to the category of most highly cited authors (top 0.5%). In 2008, he was elected by the IEEE AP Society to receive the Chen-To Tai Distinguished Educator Award. He is currently the Editor-in-Chief of the *Journal of ElectromagneticWaves and Applications/Progress in Electromagnetic Research Journal*, and on the Board of Directors of the Applied Science Technology Research Institute, Hong Kong.